Journal of Power Sources 243 (2013) 60–64

Contents lists available at SciVerse ScienceDirect

Journal of Power Sources

journal homepage: www.elsevier.com/locate/jpowsour

Short communication

Reaction mechanism of all-solid-state lithium–sulfur battery with two-dimensional mesoporous carbon electrodes

Miki Nagao [a], Yuki Imade [a], Haruto Narisawa [a], Ryota Watanabe [b], Toshiyuki Yokoi [b], Takashi Tatsumi [b], Ryoji Kanno [a,*]

[a] Department of Electronic Chemistry, Tokyo Institute of Technology, Yokohama 226-8502, Japan
[b] Chemical Resources Laboratory, Tokyo Institute of Technology, Yokohama 226-8502, Japan

HIGHLIGHTS

- Sulfur/CMK-3 composite cathode for all-solid-state battery.
- Structure and reaction mechanism of the sulfur/carbon composites were determined.
- Sulfur deposited randomly in the mesopore of the carbon by gas-phase mixing.
- Carbon stacking changed during charge–discharge reaction.
- One of two Li_2S modifications appeared during discharge participated in the reversible reaction.

ARTICLE INFO

Article history:
Received 4 March 2013
Received in revised form
7 May 2013
Accepted 11 May 2013
Available online 18 May 2013

Keywords:
Lithium–Sulfur battery
All-solid-state battery
CMK-3
Mesoporous carbon
Small-angle X-ray scattering

ABSTRACT

The reaction mechanism of all-solid-state lithium–sulfur batteries was studied by small- and wide-angle X-ray scattering. The results revealed that sulfur deposited in the electrode framework has a random distribution on the carbon wall of the highly ordered mesoporous carbon, CMK-3. Heat treatment complicated carbon surfaces with attached sulfur and improved the reversible charge–discharge reaction. Two Li_2S phases formed during the discharge reaction; one of them participates in the reversible battery reactions.

1. Introduction

Lithium–sulfur batteries are promising high-power storage devices for both small-scale portable devices and large-scale electric vehicle and stationary applications. Lithium-based systems have a high energy storage due to their low weight and high electrochemical potential. Despite its low electrical conductivity [1], sulfur is promising for use in high-capacity cathodes since it has a high theoretical capacity of 1672 mAh g^{-1} [2–5]. Moreover, since elemental sulfur has a high natural abundance, batteries based on the lithium/sulfur redox couple have the potential to be safe and inexpensive. The charge–discharge curve of a sulfur cathode with an organic liquid electrolyte contains two plateaus due to the ring-opening reaction of α-S_8 [6]. During charging and discharging, sulfur is converted into polysulfides, which are soluble in the organic liquid electrolyte; this loss of the active material in liquid electrolytes results in a poor rechargeability. This problem needs to be overcome in future lithium–sulfur batteries [2,6]. For extremely high energy density systems, all-solid-state batteries are significantly more stable and safer than batteries with liquid electrolytes [3]. We recently reported that an all-solid-state lithium–sulfur battery exhibited an extremely high capacity [7]. The charge–discharge experiments provide highly reversible capacity of 1300 mAh g^{-1} even after 20 cycles for sulfur/CMK-3 composite electrode. This high capacity was provided by an electrode framework structure composed of the highly ordered mesoporous carbon, CMK-3. The interaction between the sulfur and carbon surfaces is considered to contribute to its reversible reaction.

* Corresponding author. Tel./fax: +81 045 924 5401.
E-mail address: kanno@echem.titech.ac.jp (R. Kanno).

0378-7753/$ – see front matter © 2013 Elsevier B.V. All rights reserved.
http://dx.doi.org/10.1016/j.jpowsour.2013.05.037

In the present study, the structure of sulfur/CMK-3 composite electrodes was investigated by small-angle X-ray scattering (SAXS) and wide-angle X-ray scattering (WAXS) measurements and the charge–discharge mechanism of these composite electrodes was clarified.

2. Experimental

The mesoporous carbon, CMK-3, was synthesized from a mesoporous silica SBA-15 template [8,9]. The sulfur–carbon composite was prepared by gas-phase mixing [3]. The following mixing processes were used. Sulfur (Kojundo Chemical Laboratory; >99.99% purity) and CMK-3 were weighed in a ratio of 30:70 (weight % (wt.%)), mixed in an argon-filled glove box, sealed in a quartz tube under vacuum, and then heated at 300 °C. After heating, the tube was slowly cooled to room temperature. The composite was heated at 170–230 °C for 5 h to remove sulfur from the particle surfaces. Thio-LISICON ($Li_{3.25}Ge_{0.25}P_{0.75}S_4$) synthesized by a solid-state reaction was used as the solid electrolyte [10]. The positive electrode was fabricated from the sulfur–carbon composite and thio-LISICON ($Li_{3.25}Ge_{0.25}P_{0.75}S_4$), which were mixed with a weight ratio of 50:50 in a planetary ball mill (Fritsch, P-7). The test cell was composed of a polyethylene terephthalate cylinder with an inner diameter of 10 mm. About 70 mg of the solid electrolyte (thio-LISICON) was pressed into a pellet. Then, 5 mg of the positive electrode was pressed onto one side of the electrolyte pellet at 500 MPa. A lithium–aluminum composite was used as the negative electrode [11]. The negative electrode was a combination of 0.1-mm-thick aluminum foil and 0.1-mm-thick lithium foil (diameter: 10 mm). The Li/Al ratio was about 38/68 mol.%, which provides a potential of 0.38 V vs. Li/Li^+. The aluminum foil was attached to the solid electrolyte by applying a pressure of 500 MPa [11] and the lithium sheet was then attached to the aluminum foil. The cells were prepared and fabricated in a dry argon-filled glove box (Miwa Mfg. Co. Ltd.; [H_2O] <0.1 ppm). The electrochemical properties were characterized by a multichannel galvanostat (TOSCAT-3100, Toyo System Co. Ltd.) using currents in the range 0.013–1.3 mA cm^{-2} at 25 °C. The resistivity of the cells was examined at 1.5 V by the ac impedance method for frequencies in the range of 10 mHz–1 MHz and an applied ac voltage of 10 mV using a Solartron 1260 frequency response analyzer. These electrodes were characterized by SAXS and WAXS measurements using a Rigaku Ultima-IV with Cu Kα radiation.

3. Results and discussion

Small- and wide-angle scattering measurements

Fig. 1 shows X-ray scattering patterns for CMK-3, the sulfur/CMK-3 composite, and the sulfur/CMK-3 composite annealed at 230 °C. The SAXS and WAXS patterns are combined to clearly indicate the structural changes that occur during mixing and annealing.

Diffraction peaks in scattering patterns

The SAXS profile of CMK-3 contains several diffraction peaks around Q = 0.06–0.14 $Å^{-1}$. The peaks at Q = 0.068, 0.118, and 0.135 $Å^{-1}$ were respectively indexed as (10), (11), and (20) Bragg peaks of the two-dimensional hexagonal structure. The WAXS peaks at 1.6 and 3.1 $Å^{-1}$ correspond to the 002 and 10 Bragg peaks, respectively. Scattering from voids in the structure and carbon rods may be observed around 3–10 and 0.03–3 $Å^{-1}$, respectively. However, these scattering peaks could not be clearly observed in the present measurements since they overlap with Bragg scattering due to the carbon rod arrangement.

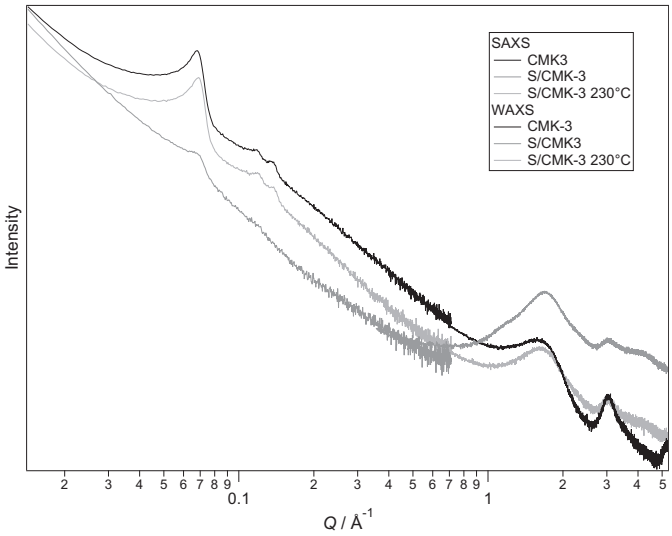

Fig. 1. X-ray scattering patterns of CMK-3, sulfur/CMK-3 composite, and sulfur/CMK-3 composite annealed at 230 °C.

Scattering at Q = 0.2–0.4 $Å^{-1}$

The slope of the SAXS profile within Q = 0.2–0.4 $Å^{-1}$ indicates the scatterer shape. In the equation, $I(Q) = AQ^p$, the slopes $p = -4$, -2, and -1 correspond to spherical, disk-shaped, and rod-shaped scatterers, respectively. The slope of CMK-3 in Fig. 1 was calculated to be -2.4, which indicates that the structure of the scattering face of CMK-3 is a swelled disk, which is intermediate between a disk and a rod. These results are consistent with the SEM images of CMK-3 [7], which reveal that the carbon has a closed packed structure in an infinitely long disk (cylinder).

Scattering at Q = 0.7–5 $Å^{-1}$

The SAXS and WAXS patterns can be expressed by the following equation [12]:

$$I = AQ^p + B_1\exp\left(\frac{-(Q-Q_1)^2}{\sigma_1^2}\right) + B_2\exp\left(\frac{-(Q-Q_1/2)^2}{\sigma_2^2}\right) + B_3\exp\left(\frac{-(Q-Q_1)^2}{\sigma_3^2}\right) + Bkg \quad (1)$$

The first term on the right-hand side of this equation gives Porod's law when $p = -4$, corresponding to scatterer with a smooth flat surface. The second to fourth terms are Gaussian functions corresponding to the Bragg peaks 002, 001, and 10, respectively. Due to the extinction rule for graphite, the 001 reflection is not usually observed; however, the patterns of CMK-3 contain the 001 peak, which probably originates from stacking faults. The 001 term is thus included in the equation. The last term, *Bkg*, is a background term. The 002, 001, and 10 Bragg reflections were accounted for when fitting the pattern.

Structure of CMK-3

Attenuated intensity curves in the larger Q range of 0.4–1.0 $Å^{-1}$ provide information about the surface conditions. The slope of the scattering fitted by Porod's law $I(Q) = AQ^p$ provides information about the surface conditions; for example, $p = -4$ corresponds to a smooth surface (Porod's law) and the fractal dimension (D_s) of the

surface is given by $D_s = 6 + p$ [13]. The p-value estimated by fitting the WAXS pattern between $Q = 0.7$ and 3.3 Å^{-1} was −3.3, so that $D_s = 2.7$ for CMK-3.

Structure of composite electrode

The intensity of the peak around $Q = 0.07$ Å^{-1} for the S/CMK-3 composite decreased with increasing sulfur content. A periodic arrangement of carbon cylinders was difficult to observe for the S/CMK-3 composite, indicating that sulfur entered the mesopores but that it did not completely fill the pores. If sulfur was uniformly distributed on the carbon surface or filled the pores, peaks due to sulfur–sulfur interference should be observed along with those due to the carbon rod arrangement. The absence of these peaks in the SAXS pattern thus indicates that sulfur was randomly distributed on the carbon.

The slope p estimated by fitting the WAXS pattern was −3.5. The slope decreased from −3.3 to −3.5 on mixing sulfur, indicating that the thickness of the interface layers on the cylinders between the carbon and the sulfur decreased with increasing coating of the carbon surface by sulfur. The intensity reduction in this region also indicates that sulfur entered the pores.

Composite electrode structure after annealing at 230 °C

The intensity of the peak around $Q = 0.07$ Å^{-1} increased after annealing at 230 °C, indicating that there is a large scattering difference between the pores and carbon. The slope p increased from −3.5 to −3.0, indicating that the complexity of the surface increased and that the surface conditions verged the combination before sulfur mixing. The amount of sulfur in the pores decreased on annealing. These results indicate a reduction in the amount of sulfur on the carbon surface. An increase in the intensity within $Q = 0.25$–0.6 Å^{-1} after annealing indicates a reduction in the amount of sulfur inside the pores. Annealing at 230 °C reduced the amount of sulfur attached to the inside and outside of the pores. However, sulfur still exists inside in the pores, which is also indicated by the results of DTA-TG and BET measurements [7].

Changes to carbon structure of carbon/sulfur composite

Fig. 2 schematically depicts the changes to the carbon structure induced by heating. With sulfur mixing at 300 °C, sulfur entered the mesopores in the carbon rods and coated the surfaces of the CMK-3 particles. The reduction in the interlayer spacing of carbon indicates that there is a strong interaction between the sulfur and the carbon at the edges of the graphene layers. With heat treatment at 230 °C, the amount of sulfur adhered to the carbon surfaces decreased while some of the sulfur in the pores evaporated. After heat treatment, the sulfur in the pores was still strongly attached to the carbon walls of the pores. The improved charge–discharge characteristics may be due to sulfur interacting strongly with the edges of the graphene layers and sulfur in the mesopores.

Structural changes to CMK-3 during charging and discharging

Fig. 3 shows XRD patterns of the S/CMK-3 composite during the first charge–discharge cycle. These patterns contained diffraction peaks from the SE layer which contacted with the cathode layer. A broad peak appeared at 11° after discharging at 1 V. The peak position, $d = 8.02$ Å, corresponds to the 001 diffraction of carbon. The appearance of the 001 diffraction indicates that the stacking sequence of layers in the c-axis direction of carbon changes from ABAB to AAAA. In addition, the distance between the graphene layers increased from 3.74 to 4.01 Å during discharging. Discharging distorts the carbon stacking structure. These results indicate that the carbon structure affects the charge–discharge process in the S/CMK-3 composite electrodes. As lithium intercalation has not been reported in carbon layers above 1 V, the strong interaction between carbon and sulfur at the edge of the graphene layer might participate in the charge–discharge reactions.

During the discharge reaction, new diffraction peaks appeared around $2\theta = 29$–$33°$ as shown in Fig. 3(b). The diffraction peaks at 30.96, 31.22, and 32.34° were observed during the early stages of discharge at 1.6 V and new diffraction peaks appeared at 29.96, 30.10, and 31.92° in the deep discharge region of 1.3 V. These peak positions correspond to those reported previously for Li_2S [14]. Fig. 4 schematically depicts the structures of these lithium sulfides. Two phases of Li_2S formed during the charge–discharge reaction in the all-solid-state batteries. These lithium sulfides are indexed here as Li_2S–A and Li_2S–B, which correspond respectively to the high-pressure 18.8 and 7.9 GPa phases. Li_2S–A remains after charging at 3 V, whereas Li_2S–B disappears; this indicates that Li_2S–B participates in the reversible battery reaction. Both phases have anti-cotunnite structures with space groups *Pnma* (18.8 GPa) and $Pn2_1a$ (7.9 GPa). The coordination environment of lithium in the $Pn2_1a$ phase is similar to the ambient pressure phase of the anti-fluorite structure. Grzechinik et al. [14] reported that a phase transition between the anti-cotunnite and anti-fluorite structures proceeded through site exchange between the nearest lithium positions. The formation of a high-pressure phase during the lithium battery reaction suggests that the strong interaction

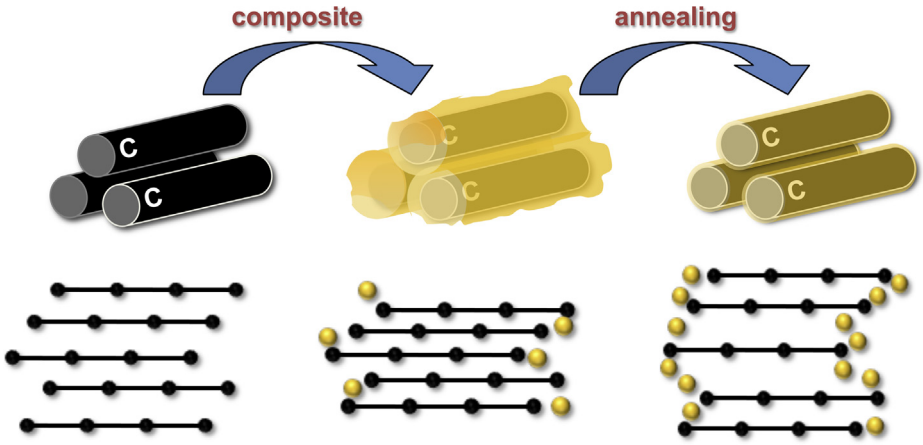

Fig. 2. Schematic diagram of carbon structural changes induced by heating.

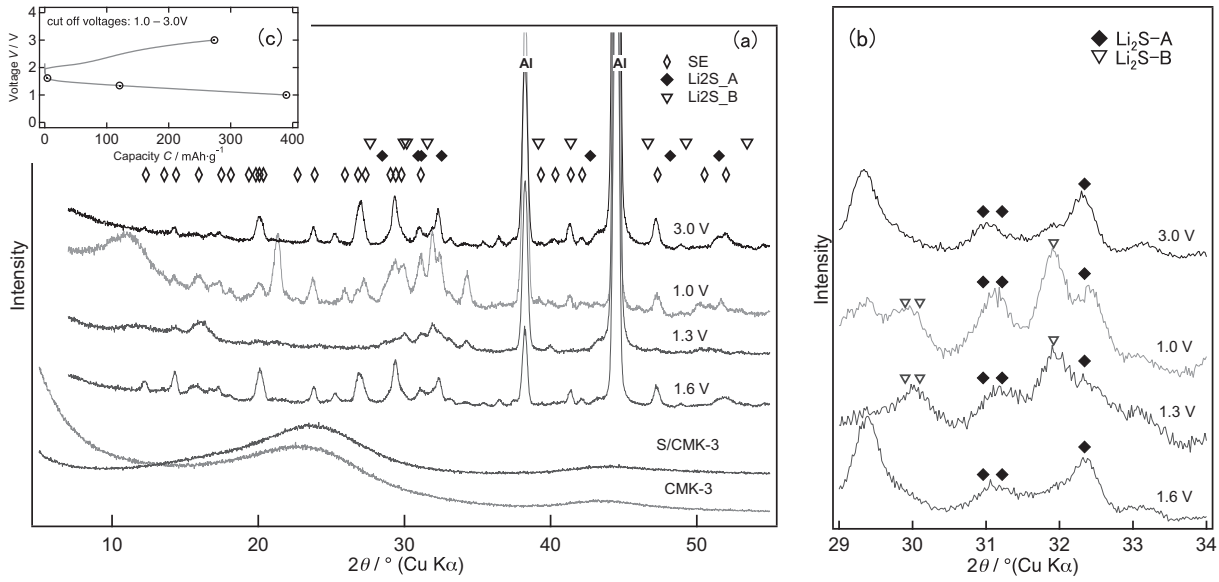

Fig. 3. (a) *Ex situ* XRD patterns for S/CMK-3 composite after discharging at 1.6, 1.3, and 1.0 V and charging at 3.0 V. (b) XRD patterns of the two Li_2S phases. (c) First discharge–charge curves of composite. Open circles indicate compositions used in *ex situ* XRD measurements.

between sulfur and grapheme edges is responsible for the formation of this phase. A strong interaction between carbon layers and intercalate ions has been proposed for a reaction in a Li–air battery [15]. Oxygen connected with the armchair edge and di-vacancy in the basal plane of carbon nanotube reacts with lithium [15]. One carbon atom at the edge and in a vacancy bond with two (2C:4O) and three (1V:3O) oxygen atoms, respectively. These carbon–oxygen bonds give rise to a high reactivity with lithium in the battery reaction. In the present lithium–sulfur system, there appears to be a strong interaction between carbon and sulfur near carbon edges. During the discharge reaction, lithium reacts with sulfur to form Li_2S with the anti-cotunnite structure in the early stages of the reaction. In the deep reaction region, another polymorph of lithium sulfide was formed; the reaction with this structure was reversible. The reaction at the deep lithiation level also changed the stacking sequence from ABAB to AAAA, which reveals that the lithiation reaction that forms Li_2S proceeded from sulfur attached to a carbon edge. The formation of an unusual polymorph of Li_2S may be due to a strong interaction between carbon and sulfur. The reaction mechanism of sulfur and lithium for all-solid-state batteries differs from those observed for liquid electrolyte systems. The cell voltages are also affected by the interaction of sulfur and carbon. The charge–discharge voltages observed for the cell with S–C composite electrode is slightly lower than that of the Li–S cell (>2 V), which indicates that the observed potential is due to a reaction between the S–C composite and lithium. The potential might therefore be dependent on the interaction between the carbon and sulfur.

Fig. 5 shows XRD patterns of the S/CMK-3 composite that had been heat treated after 100 cycles of the charge–discharge reaction. The diffraction peaks of $2\theta = 24$, 43 and 44° correspond to those of SUS, and the peaks of 38.3 and 44.5° to Al, while the peak of 72° could not be indexed. The broad diffraction peaks indicate that the sample became amorphous during the charge–discharge cycles. After 100 cycles, the 002 peak shifted to a lower angle from that of the initial S/CMK-3. The interlayer distance of about 3.9 Å is greater than that of the first discharge. These results indicate that a lithium (de-)intercalation reaction occurs in the interlayer space during

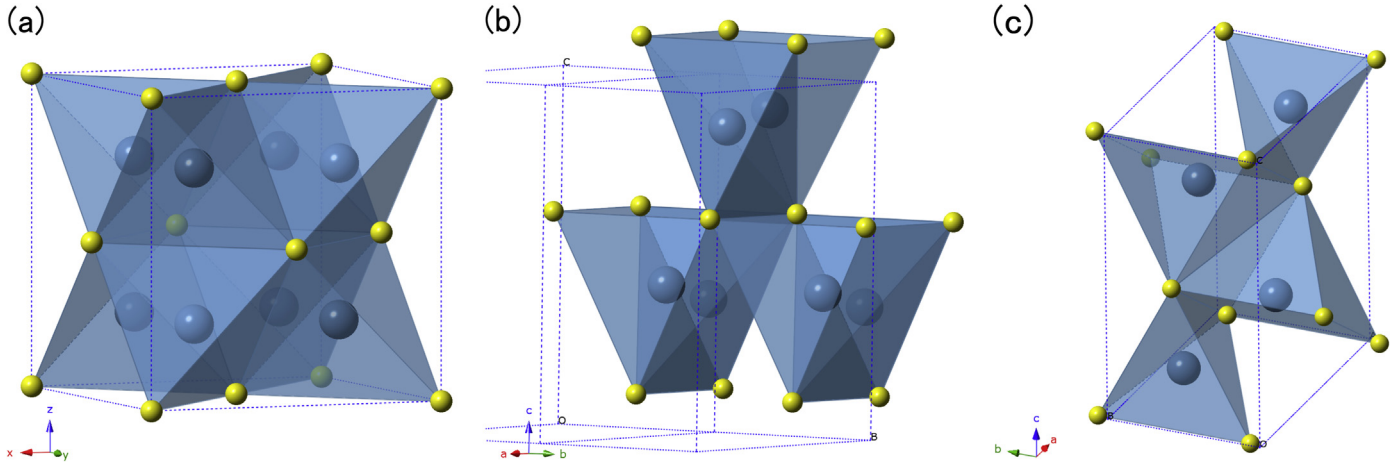

Fig. 4. Schematic diagrams of structures of Li_2S under (a) atmospheric pressure (b) 7.9 GPa, and (c) 18.8 GPa.

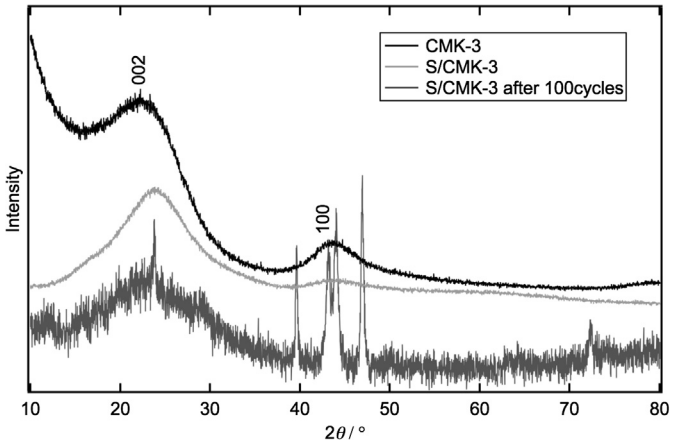

Fig. 5. XRD patterns of heat-treated S/CMK-3 composite after 100 charge–discharge cycles.

cycling. The 001 peak, which is characteristic of AAAA stacking, remains after cycling.

The charge–discharge capacity is mainly due to the reaction between sulfur and lithium. However, the interaction of lithium with the carbon matrix may increase the cell capacity above that expected based on the amount of sulfur in the carbon matrix. This is also suggested by the observed change in the cell voltages for the composite electrodes: the cell voltages are slightly lower that those for the two-phase reaction between Li_2S and S.

In the composite electrode of sulfur and mesoporous carbon, the reaction with lithium proceeds on the surface or pore of the carbons, which might change the structure of the reaction products appeared after the discharge reaction.

4. Summary

The structure of a carbon–sulfur composite was determined from X-ray scattering measurements. Sulfur entered the mesopores in carbon rods and additional sulfur that attached to the surfaces of carbon particles was removed by annealing at 230 °C. Mixing of sulfur caused sulfur to interact with the graphene sheets of the carbon matrix. In the first discharge process, sulfur reacted with lithium and two different Li_2S phases were produced in the shallow and deep lithiation regions. The former Li_2S phase was produced during the lithiation process, whereas the latter Li_2S phase, which has a different crystal structure, undergoes reversible structural changes during charging and discharging. The charge–discharge cycle caused stacking and d-spacing changes in the carbon layer, indicating a strong interaction between sulfur and the carbon layer. The carbon matrix also participates in the charge–discharge mechanism along with sulfur in the mesopores of the carbon rods. The exact capacity of the sulfur electrodes could not be calculated in the present study. Sulfur exhibited an extremely high reversibility during the charge–discharge cycles. Modifying the structure of the sulfur–carbon composite is important for improving the capacity and cycling characteristics of the sulfur electrodes.

Acknowledgment

This work is supported by the Li-ion and Excellent Advanced Batteries Development (Li-EAD) project of the New Energy and Industrial Technology Department Organization (NEDO) in Japan.

References

[1] J.A. Dean, McGraw-Hill, New York, 1985, pp. 3–5.
[2] R.D. Rauh, K.M. Abraham, G.F. Pearson, J.K. Surprenant, S.B. Brummer, J. Electrochem. Soc. 126 (1979) 523–527.
[3] T. Kobayashi, Y. Imade, D. Shishihara, K. Homma, M. Nagao, R. Watanabe, T. Yokoi, A. Yamada, R. Kanno, T. Tatsumi, J. Power Sources 182 (2008) 621–625.
[4] J. Wang, S.Y. Chew, Z.W. Zhao, S. Ashraf, D. Wexler, J. Chen, S.H. Ng, S.L. Chou, H.K. Liu, Carbon 46 (2008) 229–235.
[5] X. Ji, K.T. Lee, L.F. Nazar, Nat. Mater. 8 (2009) 500–506.
[6] J. Shim, K.A. Striebel, E.J. Cairns, J. Electrochem. Soc. 149 (2002) A1321–A1325.
[7] M. Nagao, Y. Imade, H. Narisawa, T. Kobayashi, R. Watanabe, T. Yokoi, T. Tatsumi, R. Kanno, J. Power Sources 222 (2013) 237–242.
[8] S. Jun, S.H. Joo, R. Ryoo, M. Kruk, M. Jaroniec, Z. Liu, T. Ohsuna, O. Terasaki, J. Am. Chem. Soc. 122 (2000) 10712–10713.
[9] L. Wang, S. Lin, K. Lin, C. Yin, D. Liang, Y. Di, P. Fan, D. Jiang, F.-S. Xiao, Micropor. Mesopor. Mater. 85 (2005) 136–142.
[10] R. Kanno, M. Murayama, J. Electrochem. Soc. 148 (2001) A742–A746.
[11] R. Kanno, M. Murayama, T. Inada, T. Kobayashi, K. Sakamoto, N. Sonoyama, A. Yamada, S. Kondo, Electrochem. Solid-State Lett. 7 (2004) A455–A458.
[12] M. Nagao, C. Pitteloud, T. Kamiyama, T. Otomo, K. Itoh, T. Fukunaga, K. Tatsumi, R. Kanno, J. Electrochem. Soc. 153 (2006) A914–A919.
[13] H.D. Bale, P.W. Schmidt, Phys. Rev. Lett. 53 (1984) 596–599.
[14] A. Grzechnik, A. Vegas, K. Syassen, I. Loa, M. Hanfland, M. Jansen, J. Solid State Chem. 154 (2000) 603–611.
[15] Y. Xu, W.A. Shelton, J. Electrochem. Soc. 158 (2011) A1177–A1184.